Gamma-Ray Emission from the Broad-Line Radio Galaxy 3C 111

R. C. Hartman[1], M. Kadler[2,3,4], and J. Tueller[1]

Robert.C.Hartman@nasa.gov, mkadler@milkyway.gsfc.nasa.gov, Jack.Tueller@nasa.gov

ABSTRACT

The broad-line radio galaxy 3C 111 has been suggested as the counterpart of the γ–ray source 3EG J0416+3650. While 3C 111 meets most of the criteria for a high-probability identification, like a bright flat-spectrum radio core and a blazar-like broadband SED, in the Third EGRET Catalog, the large positional offset of about 1.5° put 3C 111 outside the 99% probability region for 3EG J0416+3650, making this association questionable. We present a re-analysis of all available archival data for 3C 111 from the EGRET archives, resulting in detection of variable hard-spectrum high-energy γ–ray emission above 1000 MeV from a position close to the nominal position of 3C 111, in three separate viewing periods (VPs), at a 3σ level in each. A second variable hard-spectrum source is present nearby. At >100 MeV, one variable soft-spectrum source seems to account for most of the EGRET-detected emission of 3EG J0416+3650. A follow-up *Swift* UVOT/XRT observation reveals one moderately bright X–ray source in the error box of 3EG J0416+3650, but because of the large EGRET position uncertainty, it is not certain that the X–ray and γ–ray sources are associated. Another *Swift* observation near the second (unidentified) hard γ–ray source detected no X–ray source nearby.

Subject headings: gamma rays: observations — galaxies: active — galaxies: individual(3C 111)

1. Introduction

One of the main scientific goals of the upcoming γ–ray astronomy satellite mission GLAST (Ritz 2007; Michelson 2007) is to shed light on the nature of powerful relativistic extragalactic jets, which are ejected from the nuclei of some active galaxies (AGN). Originally, this class of AGN was defined based on the bright and prominent radio emission from these jets: the radio-loud population of active galaxies. Based on data from EGRET, the high-energy γ–ray telescope on the *Compton Gamma Ray Observatory*, it was realized (Fichtel 1994; Thompson et al. 1994) that the largest population of extragalactic ∼GeV γ–ray sources is represented by those radio-loud AGN whose jets are pointed at a small angle to the line of sight. The fact that the bright compact radio emission of these so-called blazars makes excellent targets for parsec-scale resolution very-long-baseline interferometric (VLBI) observations of their jet structure ties an intimate link between radio VLBI and high-energy γ–ray astronomy.

Of special interest are the questions of where in the AGN jets the bright γ–ray emission is produced, and how the emission is interacting with its immediate environment and with other parts of the jet. This knowledge would enable us to put crucial constrains on the processes of jet formation, collimation, and acceleration. GLAST is expected to yield densely sampled γ–ray light curves of hundreds of extragalactic jets that are bright enough to be detected on time scales of days to weeks, and thousands on time scales of months to years. Most of these objects will be blazars; in fact, all but two of the firmly identified extragalactic EGRET sources (LMC, Sreekumar et al.

[1] Astrophysics Science Division, NASA's Goddard Space Flight Center, Greenbelt, MD 20771, USA

[2] Dr. Karl Remeis-Observatory, University of Erlangen-Nuremberg, Sternwartstrasse 7, 96049 Bamberg, Germany

[3] CRESST/NASA Goddard Space Flight Center, Greenbelt, MD 20771, USA

[4] Universities Space Research Association, 10211 Wincopin Circle, Suite 500 Columbia, MD 21044, USA

1992; Centaurus A, Sreekumar et al. 1999) are blazars. In contrast to those, radio galaxies have larger inclination angles and the beaming is therefore weaker. That allows better (deprojected) linear resolution with VLBI observations and in the case of stratified jet structures, it allows observations of the slower jet layers, e.g., a sheath, whose emission may be swamped by the much brighter beamed emission from faster jet regions, e.g. a fast spine, in blazars. Ghisellini et al. (2005) have presented such a spine-sheath stratified-jet model, predicting detectable γ–ray emission from the nuclei of some radio galaxies. In their model, each of the two emission regions sees photons coming from the other part relativistically enhanced because of the relative speed difference, giving rise to an additional inverse-Compton emission component.

In this letter, we report on the identification of the broad-line radio galaxy 3C 111 as a γ–ray source, responsible for a portion of the source 3EG J0416+3650. Such an association was suggested as possible in the third EGRET catalog (Hartman et al. 1999, 3EG), but was considered unlikely because of the large positional offset of 3C 111 from 3EG 0416+3650. The present work was stimulated by the recent report of Sguera et al. (2005), who used multiwavelength data to strengthen the case for the association between 3C 111 and 3EG 0416+3650.

Using detailed analysis of reprocessed EGRET data (Esposito et al. 1999; Bertsch et al. 2001), we show here that 3EG J0416+3650 is most likely composed of at least two, and more likely three, separate sources, one of which is in good positional agreement with 3C 111. As demonstrated recently, based on VLBA monitoring data at $\lambda 2$ cm from the MOJAVE program (Kadler et al. 2008), the parsec-scale jet of 3C 111 shows a variety of physically different regions in a relativistic extragalactic jet, such as a compact core, superluminal jet components, recollimation shocks and regions of interaction between the jet and its surrounding medium, which are all possible sites of γ–ray production. Its relatively large inclination angle of $\sim 19°$ makes 3C 111 a particularly well-suited target for tests of structured-jet models, such as the model of Ghisellini et al. (2005). We describe our re-analysis of the available EGRET data on 3C 111 in Sect. 2 and discuss our results and their implications in Sect. 3.

2. Analysis

2.1. EGRET Data Analysis

We have investigated the possibility that 3EG J0416+3650 is a superposition of at least two sources, one being at or near the position of 3C 111. The analysis for 3EG was based on photons with energies >100 MeV, for which the 68% containment angle of the spectrum-dependent point spread function (PSF) is always several degrees. For energies >1000 MeV, the PSF is considerably smaller, slightly less than one degree. On the other hand, the number of photons with energies above 1000 MeV is much smaller than that above 100 MeV. Both of those integral energy ranges were investigated for this study.

For each viewing period (VP) in which 3C 111 and 3EG J0416+3650 were in the field of view (FoV) of EGRET, the following procedure was initially used:

1. Using the standard EGRET likelihood software (LIKE), two sources were modeled, one at the 3EG position for 3EG J0416+3650 and one at the nominal position of 3C 111, and LIKE then provided the best estimates of the significance and flux of the two assumed sources.

2. If either of the two assumed sources had a test statistic (TS) of at least 2.5 (roughly 1.6σ), LIKE was then allowed to optimize the significance of the two sources by moving their positions.

The results from this procedure are shown in Table 1, for the two energy ranges and the two assumed sources. The first five columns show the VPs, the starting dates of the observations, the lengths of the VPs, EGRET wide (W) or narrow (n) FoV mode, and the off-axis angle of 3C 111. The line showing VP=P1234 is the analysis of the summed data for the VPs included in 3EG, VP0002 through VP4270. The EGRET team has normally used data out to 19° in narrow-field mode, but as indicated in Column 5, that limit was stretched for the present study. This means that we were using regions of very low exposure, with possible slight systematic distortion of positions (Esposito et al. 1999). For each source and energy range, the table shows the TS at the starting

position, the change in position (from the starting point) to obtain the maximum TS, and the resulting photon flux in units of 10^{-8} photons cm^{-2} s^{-1}. Blank entries for TS indicate values of 0.00. For TS values less than 2.5 (roughly 1.6σ significance), there are no entries in the next two columns.

The density of detections in this table is very low, even with the low requirement of TS$\geq$2.5. Three of the 3C 111 detections (P1234 and VP4270 for E$>$100 MeV and VP0150 for E$>$1000 MeV) have offset position values larger than would be expected, and out of line with the other detections. The VP0002 detection ($>$100 MeV) of J0416 is probably suspect for the same reason.

Only one VP (3211) provides a reasonably strong detection of 3EG J0416+3650, which agrees well with the information provided in 3EG. The summed exposure P1234 provides about the same significance of detection, indicating that the object was emitting γ rays at a low level even when it was not significantly detectable in individual VPs. The two weak detections of 3EG J0416+3650 at E$>$1000 MeV (VP4270 and P1234) agree well in position with the E$>$100 MeV, but show very low photon fluxes.

After excluding the suspect detections, there are six VPs that support the proposed 3C 111 γ–ray source, three in E$>$100 MeV and three in E$>$1000 MeV. In each of these six cases, the value of offset in position is compatible (considering the energy range) with the position of 3C 111. Only one VP (0310) shows detections in both energy ranges; however, each of the detections in that VP is the strongest in its energy band. Like 3EG J0416+3650, 3C 111 appears to radiate γ rays with a low duty cycle, occasionally becoming fairly bright. Note that the best exposure, VP0390, does not show detection of either of the two assumed sources.

The number of photons $>$100 MeV from 3C 111 was 64, 44 of them in VP0310. Only about 14 photons $>$1000 MeV were detected from 3C 111, six in VP0150, four in VP0310, and four in VP3250. For 3EG J0416+3650, there was a total of 152 photons $>$100 MeV, 40 of them in VP3211, the most significant single detection. P1234 yielded seven photons above 1000 MeV from 3EG J0416+3650, but as indicated in Table 1, they produced a TS of only 3.43, about 1.8σ.

We have further investigated a small region around 3EG J0416+3650 by generating $5° \times 5°$ likelihood maps, for the energy ranges $>$100 MeV and $>$1000 MeV, for each VP in which 3C 111 and 3EG J0416+3650 were in the FoV. A sample of the more informative likelihood maps is shown in Figure 1. Maps for the summed data, P1234, are shown in Figure 2. We draw the following conclusions from these maps:

1. There appear to be at least three sources (possibly more) contributing, two in the $>$1000 MeV energy range and at least one in the $>$100 MeV range. One of the two $>$1000 MeV sources is very near the position of 3C 111; for the other, which is of comparable strength, we find no obvious identification (see below). In the following, we designate this source EGEV J0426+3747.

2. The two $>$1000 MeV sources appear to have very hard spectra, since there is little or no significant emission detected in the lower energy bands.

3. The $>$100 MeV emission is dominated by a source near the 3EG catalog position. This source seems to have a very soft spectrum, since there is no significant detection in the $>$1000 MeV energy range. In the following, the name 3EG J0416+3650 refers implicitly to this soft source.

4. The duty cycle of all three sources seems to be in the range 10-25%.

5. The $>$1000 MeV map for VP0150 shows why the position offset for 3C 111 is so large (0.423°) in Table 1 in that VP. There are only about seven photons near 3C 111 in that map. One of them is nearly a degree away from 3C 111. This shifts the maximum likelihood position toward that single photon, which could be either from the tail of the PSF, or from the diffuse Galactic foreground. Thus this VP, which had previously been ignored, provides additional support for the $>$1000 MeV detection of 3C 111.

As an additional check on the reality of the two $>$1000 MeV sources, we have compared the number of occurrences of $\geq$2σ excesses in 17 maps

3

TABLE 1

EGRET OBSERVATIONS OF 3C 111 AND 3EG 0416+3650 ANALYZED IN THIS STUDY.

VP	Start Date	Days	FoV	Off-Axis[a] [deg]	>100 MeV 3C 111 TS[c]	Offset [deg]	Flux[b]	J 0416+3650 TS[d]	Offset [deg]	Flux[b]	>1000 MeV 3C 111 TS[c]	Offset [deg]	Flux[b]	J 0416+3650 TS[d]	Offset [deg]	Flux[b]
0002	04-22-1991	6	W	24.82		-		12.14	1.196	50		-		0.88	-	
0005	05-04-1991	3	W	22.82	0.15	-		1.21	-			-			-	
0010	05-16-1991	14	W	29.31		-			-			-			-	
0150	11-28-1991	14	W	10.01	0.04	-		2.91	0.299	8	8.96	0.423	2.0	0.19	-	
0310	06-11-1992	14	W	20.79	10.01	0.19	26	0.55	-		8.86	0.188	3.2		-	
0365	08-12-1992	8	W	6.44	1.64	-		0.73	-			-			-	
0390	09-01-1992	16	W	5.45		-		1.58	-		1.30	-		0.03	-	
2130	03-23-1993	6	W	20.72		-		0.42	-			-			-	
2210	05-13-1993	11	W	25.79	0.66	-			-			-			-	
3211	02-08-1994	7	W	20.60		-		16.90	0.185	55		-		2.41	-	
3215	02-15-1994	2	W	20.60	6.76	0.45	64		-			-			-	
3250	04-26-1994	14	W	14.47	1.71	-			-		4.14	0.092	2.3	0.78	-	
4120	02-28-1995	7	W	25.41	0.16	-			-			-		0.25	-	
4260	08-08-1995	14	W	22.82		-		0.94	-			-			-	
4270	08-22-1995	16	W	7.91	2.98	1.85	20	0.13	-		0.20	-		3.81	0.049	1.1
P1234	–	–	W	—	2.73	1.22	4	16.48	0.064	10	8.59	0.109	0.8	3.43	0.031	0.5
5020	10-17-1995	14	n	28.65		-		0.74	-			-			-	
7289	10-13-1998	21	n	23.80		-		-	-			-			-	
8290	09-14-1999	14	n	21.13	4.06	0.08	77		-			-			-	
9185	04-25-2000	14	W	25.65	0.09	-			-		0.31	-			-	

[a]Off-axis angle for the position of 3C 111

[b]Flux in units of $10^{-8}\,\mathrm{ph\,cm^{-2}\,s^{-1}}$

[c]Test statistic at the position of 3C 111

[d]Test statistic at the position of 3EG J0416+3650

(5° by 5°) with the statistically expected value. The results are shown in Table 2. For the regions of the maps away from the two "source" positions, the number of $>2\sigma$ excesses is about as expected from statistical fluctuations, taking into account the number of PSFs contained within each map. Near the locations of the two $>1000\,\mathrm{MeV}$ sources, however, there are far more excesses than expected, which provides added confidence in the detections of 3C 111 and EGEV J0426+3747.

2.2. *Swift* Follow-Up X-Ray Observations and Their Analysis

There are no known high-energy sources close to the nominal best-fit positions of 3EG J0416+3650 and EGEV J0426+3747. Therefore, we have conducted follow-up optical/UV and X-ray observations with the UVOT and XRT instruments on the NASA satellite *Swift* (Gehrels et al. 2004). The 3EG J0416+3650 field was observed with XRT for 10.4 ksec on December 14, 2007[2], and the EGEV J0426+3747 field for 9.0 ksec on 20 December, 2007[3]. No significant X-ray source was detected in the 23.6×23.6 arcsec XRT FoV around EGEV 0426+3747 above the background count rate level of $0.00045\,\mathrm{cts\,s^{-1}}$. The XRT observation of the 3EG J0416+3650 field detected one 4.8σ source at the position 04 h 15 m 54.3 s, +36 d 49 m 26 s, with an uncertainty of 5.8 arcsec. Despite the fact that this position is very close to the best position estimate for 3EG 0416+3650, the large position uncertainty of the EGRET source precludes a firm association between them.

We extracted spectra from the source (which we designate Swift J041554.3+364926) and background regions using XSELECT, and response and ancillary files provided by the *Swift* calibration data base (CALDB)[4]. The low count rate of $0.0026 \pm 0.0006\,\mathrm{cts/s^{-1}}$ limits the ability to derive spectral information. However, it is striking that only 4 photons (out of 26) have been detected between 0.2 keV and 1 keV. To characterize the spectrum, we used Cash statistics (Cash 1979) in XSPEC and determined the maximum allowable power-law photon index in a power-law fit under the assumption of zero absorption. The result is

slightly dependent on the data binning chosen, but suggests a very hard spectrum, with the photon index in the range 1.1-1.3. If absorption is allowed, the photon index is poorly constrained, and steeper values up to 2.7 are statistically allowed.

2.3. Spectral energy distributions

The non-contemporaneous spectral energy distribution (SED) of 3C 111 is shown in Figure 3. The millimeter flux range was determined (with permission) from the SMA Submillimeter Calibrator List archived data[5] (Gurwell et al. 2007). The R-band flux range has been determined from data obtained in a long-term monitoring program with the Liverpool telescope (PI: I. McHardy) between November 2004 and July 2007 (S. Jorstad, priv. communication).

The 3C 111 SED is similar to those of EGRET-detected flat-spectrum radio quasars (FSRQs), except that the rollover in the NIR, optical, and UV is steeper here. This makes the "valley" between the synchrotron and Compton "bumps" appear deeper. This could be due to absorption, but it must be intrinsic to 3C 111, since the data points have been corrected for local absorption.

Figure 4 shows (a) a UVOT image of the Swift J041554.3+364926 region, with a circle containing the XRT X-ray photons superimposed; and (b) an SED containing the very limited data available. The EGRET points shown are for comparison only; despite its proximity to the 3EG position for the γ-ray source, it is not certain that Swift J041554.3+364926 is actually the same object as 3EG J0416+3650, because the EGRET position uncertainty is quite large (about 0.63° in radius). Furthermore, 3EG J0416+3650 is quite variable, and in the SDSS POSS-I Blue Survey image from a 1955 Palomar plate, there is an additional object present about 25 arcsec west of Swift J041554.3+364926 (at 04:15:52.411; +36:49:24.77). This object does not appear in any other optical or IR image we have located.

In the Swift J041554.3+364926 SED, the UVOT data are plotted twice, with and without dereddening, because it is not certain whether the object is nearby or extragalactic. The open circles

---

TABLE 2

EXCESSES $\geq 2\sigma$ IN 17 MAPS (5° BY 5°) OF THE FIELD AROUND 3EG J0416+3650.

VP	Full Field[a]	3C 111 Field[b]	0426+3747 Field[c]	Background Field[d]
0002	0	0	0	0
0005	s	0	s	0
0010	1	0	0	1
0150	2	1	1	0
0310	1	1	0	0
0360	1	0	0	1
0365	0	0	0	0
0390	1	0	0	1
2130	1	0	0	1
2210	1	0	1	1
3211	2	0	1	1
3215	s	0	s	0
3250	4	1	1	2
4120	2	0	0	2
4260	0	0	0	0
4270	1	0	0	1
8290	1	0	1	0
Sum	$18 + 2s$	3	$5 + 2s$	11
Rate	10%	18%	29%	7%

NOTE.— s (in VPs 0005, 3215, columns 2 and 4) - a single photon >1000 MeV very near the source position, significant because of the short exposures; [a] 187 PSFs; [b] 17 PSFs; [c] 17 PSFs; [d] 153 PSFs

TABLE 3

3C 111 HISTORICAL SED DATA

Frequency[a]	Band	Instrument	Flux[b]	Flux Error	Reference
$(0.24 - 24.1) \times 10^{23}$	$> 100\,\mathrm{MeV}$	EGRET(max)	1.92×10^{-10}	7.07×10^{-11}	this work
$(2.41 - 24.1) \times 10^{23}$	$> 1000\,\mathrm{MeV}$	EGRET(max)	1.11×10^{-10}	7.00×10^{-11}	"
$(2.41 - 24.1) \times 10^{23}$	$> 1000\,\mathrm{MeV}$	EGRET(avge)	2.90×10^{-11}	1.50×10^{-11}	"
$(0.24 - 24.1) \times 10^{23}$	$> 100\,\mathrm{MeV}$	EGRET(avge)	3.00×10^{-11}	1.90×10^{-11}	"
$(0.24 - 24.1) \times 10^{23}$	$> 100\,\mathrm{MeV}$	EGRET(VP3215)	4.28×10^{-10}	2.06×10^{-10}	"
$(2.41 - 24.1) \times 10^{23}$	$> 1000\,\mathrm{MeV}$	EGRET(VP3215)	$< 1.53 \times 10^{-10}$		"
$(2.41 - 7.23) \times 10^{20}$	$1 - 3\,\mathrm{MeV}$	COMPTEL	$< 1.30 \times 10^{-10}$		Maisack et al. (1997)
$(7.23 - 24.1) \times 10^{20}$	$3 - 10\,\mathrm{MeV}$	COMPTEL	$< 1.30 \times 10^{-10}$		"
$(2.41 - 7.23) \times 10^{21}$	$10 - 30\,\mathrm{MeV}$	COMPTEL	$< 3.00 \times 10^{-10}$		"
$(1.81 - 2.41) \times 10^{20}$	$0.75 - 1\,\mathrm{MeV}$	COMPTEL	$< 2.90 \times 10^{-10}$		"
$(1.20 - 3.60) \times 10^{19}$	$50 - 150\,\mathrm{keV}$	OSSE	3.52×10^{-11}	6.56×10^{-12}	Johnson et al. (1997)
$(9.70 - 24.0) \times 10^{18}$	$40 - 100\,\mathrm{keV}$	ISGRI	8.10×10^{-11}	7.40×10^{-12}	Beckmann et al. (2006)
$(4.80 - 9.70) \times 10^{18}$	$20 - 40\,\mathrm{keV}$	ISGRI	6.27×10^{-11}	5.70×10^{-12}	"
$(3.39 - 47.2) \times 10^{18}$	$14 - 195\,\mathrm{keV}$	BAT	1.25×10^{-10}	9.00×10^{-12}	Tueller et al. (2007)
$(4.80 - 19.3) \times 10^{18}$	$2 - 80\,\mathrm{keV}$	BeppoSax	4.99×10^{-11}	9.98×10^{-12}	Kadler (2005); Kadler et al. (2008)
$(4.80 - 24.0) \times 10^{17}$	$2 - 10\,\mathrm{keV}$	BeppoSax	2.49×10^{-11}	4.98×10^{-12}	"
$(1.20 - 4.80) \times 10^{17}$	$0.5 - 2\,\mathrm{keV}$	BeppoSax	4.36×10^{-12}	8.72×10^{-13}	"
$(4.80 - 24.0) \times 10^{17}$	$2 - 10\,\mathrm{keV}$	XMM	6.57×10^{-11}	3.94×10^{-13}	"
$(1.20 - 4.80) \times 10^{17}$	$0.5 - 2\,\mathrm{keV}$	XMM	1.38×10^{-11}	3.94×10^{-13}	"
$(4.80 - 24.0) \times 10^{17}$	$2 - 10\,\mathrm{keV}$	ASCA	3.92×10^{-11}	7.84×10^{-12}	"
$(1.20 - 4.80) \times 10^{17}$	$0.5 - 2\,\mathrm{keV}$	ASCA	7.42×10^{-12}	1.48×10^{-12}	"
1.14×10^{15}	UVW1	UVOT	$< 6.98 \times 10^{-13}$		F. Verrecchia, priv. comm.
8.57×10^{14}	U	UVOT	$< 6.95 \times 10^{-13}$		"
6.92×10^{14}	B	UVOT	1.00×10^{-12}	$(+1.0, -0.5) \times 10^{-12}$	"
5.55×10^{14}	V	UVOT	2.30×10^{-12}	$(+1.1, -0.7) \times 10^{-13}$	"
4.29×10^{14}	R	Liverpool	$(4.22 - 7.25) \times 10^{-12}$		S. Jorstad, priv. comm.
2.40×10^{14}	J	2MASS	1.19×10^{-11}	4.00×10^{-13}	2MASS archive Skrutskie et al. (2006)
1.82×10^{14}	H	2MASS	1.59×10^{-11}	4.62×10^{-13}	"
1.36×10^{14}	K	2MASS	1.92×10^{-11}	3.66×10^{-13}	"
2.50×10^{13}	12 micron	IRAS	2.43×10^{-11}	3.65×10^{-12}	Golombek et al. (1988)
1.20×10^{13}	25 micron	IRAS	2.69×10^{-11}	4.04×10^{-12}	"
5.00×10^{12}	60 micron	IRAS	1.61×10^{-11}	2.42×10^{-12}	"
3.40×10^{11}	0.85 mm	SMA	$(28.4 - 5.27) \times 10^{-12}$		SMA archive[1]
2.30×10^{11}	1.3 mm	SMA	$(25.9 - 0.94) \times 10^{-12}$		"
9.00×10^{10}	3 mm	SMA	$(3.66 - 0.91) \times 10^{-12}$		"
1.50×10^{10}	2 cm	UMRAO	$(1.05 - 0.30) \times 10^{-12}$		Kadler et al. (2008)
8.00×10^{09}	3.6 cm	UMRAO	$(6.40 - 3.20) \times 10^{-13}$		"
5.00×10^{09}	6 cm	UMRAO	$(4.50 - 3.00) \times 10^{-13}$		"

[a]Frequency in units of Hz

[b]Flux in units of $\mathrm{erg\,cm^{-2}\,s^{-1}}$

TABLE 4

3EG J 0416+3650 SED DATA

Frequency[a]	Band	Instrument	Flux[b]	Flux Error	Reference
$(0.24 - 24.1) \times 10^{23}$	$> 100\,\mathrm{MeV}$	EGRET(avge)	7.03×10^{-11}	1.89×10^{-11}	this work
$(0.24 - 24.1) \times 10^{24}$	$> 100\,\mathrm{MeV}$	EGRET(VP3211)	4.42×10^{-10}	1.29×10^{-10}	"
$(3.39 - 47.2) \times 10^{18}$	$14 - 195\,\mathrm{keV}$	BAT	$< 1.78 \times 10^{-11}$		Tueller et al. (2007)
$(4.82 - 24.1) \times 10^{17}$	$2 - 10\,\mathrm{keV}$	XRT	1.05×10^{-13}	5.24×10^{-14}	this work
1.48×10^{15}	UVW2	UVOT(observed)	4.43×10^{-14}	1.48×10^{-14}	"
1.34×10^{15}	UVM2	UVOT(observed)	5.38×10^{-14}	1.35×10^{-14}	"
1.14×10^{15}	UVW1	UVOT(observed)	1.94×10^{-13}	2.28×10^{-14}	"
8.57×10^{14}	U	UVOT(observed)	7.80×10^{-13}	3.43×10^{-14}	"
6.93×10^{14}	B	UVOT(observed)	9.29×10^{-13}	5.57×10^{-14}	"
5.55×10^{14}	V	UVOT(observed)	1.13×10^{-12}	9.40×10^{-14}	"
1.48×10^{15}	UVW2	UVOT(dereddened)	5.16×10^{-12}	1.72×10^{-12}	"
1.34×10^{15}	UVM2	UVOT(dereddened)	8.06×10^{-12}	2.02×10^{-12}	"
1.14×10^{15}	UVW1	UVOT(dereddened)	6.25×10^{-12}	7.38×10^{-13}	"
8.57×10^{14}	U	UVOT(dereddened)	1.06×10^{-11}	4.67×10^{-13}	"
6.93×10^{14}	B	UVOT(dereddened)	8.15×10^{-12}	4.89×10^{-13}	"
5.55×10^{14}	V	UVOT(dereddened)	6.22×10^{-12}	5.17×10^{-13}	"
4.29×10^{14}	R	2MASS	$< 4.58 \times 10^{-12}$		2MASS archive Skrutskie et al. (2006)
2.40×10^{14}	J	2MASS	2.66×10^{-12}	2.66×10^{-13}	"
1.82×10^{14}	H	2MASS	1.73×10^{-12}	2.60×10^{-13}	"
1.36×10^{14}	K	2MASS	1.57×10^{-12}	1.57×10^{-13}	"
1.40×10^{09}	20 cm	NVSS	$< 1.40 \times 10^{-17}$		Condon et al. (1998)

[a] Frequency in units of Hz

[b] Flux in units of $\mathrm{erg\,cm^{-2}\,s^{-1}}$

denote the observed fluxes; the dereddened fluxes are shown as filled circles. Note that the fall-off in the optical-UV is extremely steep, especially in the observed fluxes. If Swift J041554.3+364926 is an extragalactic source, this can be attributed to absorption in a fairly dense foreground molecular cloud, part of the Taurus complex, with absorbing column density $N_\mathrm{H} = 2.18 \times 10^{21}\,\mathrm{cm^{-2}}$ (Kalberla et al. 2005). NED shows A_V of 1.893m for the catalog position of the EGRET source, about 0.1° away. In the extragalactic scenario, Swift J041554.3+364926 must be a radio quiet source because of the very low upper limit on its radio flux density, 0.7 mJy at 1.4 GHz, from the NVSS survey (Condon et al. 1998). The shape of the dereddened UV/optical/IR range suggests an AGN "blue bump", usually attributed to thermal emission from an accretion disk. However, without far IR and/or submillimeter data points, it is not possible to be certain of this interpretation. Based on previous experience, a radio-quiet AGN is an unlikely identification for an EGRET source.

Alternatively, if Swift J041554.3+364926 is within our Galaxy, it would need to be an M star or a cataclysmic variable (CV) in order to produce the observed X-rays (R. Osten and S. Drake, personal communication). In order to be visible optically, an M star would necessarily be in front of the molecular cloud, which is 140 pc distant (Elias 1978), so the observed UVOT data points should be considered, rather than the dereddened ones. The observed X-ray emission is stronger than expected from an M star except during an exceptional flare (R. Osten and S. Drake, personal communication). If the object is a CV, its luminosity is much greater, so it must be behind the Taurus absorber, making the dereddened UVOT points appropriate; in that case the X-ray emission is reasonable. Based on previous experience, neither an M star or a CV would be a likely identification for an EGRET source.

Table 3 and Table 4 provide the values plotted in Figures 3 and 4, with references.

3. Conclusions

The 3EG source 3EG J0416+3650 seems to be composed of at least three highly variable sources, two hard-spectrum (3C 111 and EGEV J0426+3747)

and one soft-spectrum. One of the hard-spectrum sources is close to the radio galaxy 3C 111, and presumably associated with it; the other, EGEV J0426+3747, has no obvious identification at other wavelengths. The soft-spectrum gamma-ray source may be associated with the XRT source Swift J041554.3+364926. The region under study is $8 - 10°$ from the Galactic plane, so one or both of these additional sources could be local.

Our re-analysis of the available EGRET data supports the previous association of 3EG J0416+3650 with the broad line radio galaxy 3C 111, but with 3C 111 responsible for only a portion of the γ–ray emission. Furthermore, it explains the relatively large positional offset noted in Hartman et al. (1999). We have compiled a historical SED of 3C 111 which shows that the X–ray data may well extrapolate into the EGRET range, particularly during flares, which is in agreement with the intermittent nature of detections in the individual EGRET viewing periods. It is interesting to note that we detect 3C 111 at almost exactly the gamma-ray flux that is predicted by equation (12) in Ghisellini et al. (2005): $(1.41 - -14.1) \times 10^{-11}\,\mathrm{erg\,s^{-1}\,cm^{-2}}$, scaling from the 5 GHz values in Table 3. Note that 3C 111 (z=0.0485) is the most distant radio galaxy detected in γ rays, about twice as far as NGC 6251 (Mukherjee, Halpern, & Mirabal; z=0.0247).

The detection of strong and variable gamma-ray emission from 3C 111 further supports the hypothesis that radio galaxies may represent an important class of GLAST sources. GLAST's LAT detector is about a factor of 30 more sensitive than EGRET, with a factor of $\sim$3 better PSF above 1 GeV. It is scheduled for launch in mid-May, 2008, and will continuously scan the entire sky, so it will be far more sensitive to transient events than EGRET. In the case of 3C 111, EGEV J0426+3747, and Swift J041554.3+364926, the smaller PSF of the LAT will clearly separate these three sources and allow us to measure their time-variable gamma-ray spectra and duty cycles.

REFERENCES

Beckmann, V., Gehrels, N., Shrader, C. R., & Soldi, S. 2006, ApJ, 638, 642

Bertch, D. L., Hartman, R. C., Hunter, S. D., Thompson, D. J., & Sreekumar, P. 2001, in AIP Conf. Proc.587, Gamma 2001, ed. Ritz, S., Gehrels, N., & Shrader, C. R. (Melville, NY: AIP), 706

Cash, W. 1979, ApJ, 228, 939

Condon, J. J., Cotton, W. D., Greisen, E. W., Yin, Q. F., Perley, . A., Taylor, G. B., & Broderick, J. J. 1998, AJ, 115, 1693

Dadina, M. 2007, A&A, 461, 1209

Elias, J. H. 1978, ApJ, 224, 857

Esposito, J. A., et al. 1999, ApJS, 123, 203

Fichtel, C. E. 1994, ApJS, 90, 917

Gehrels, N., et al. 2004, ApJ, 611, 1005

Ghisellini, G., Tavecchio, F., & Chiaberge, M. 2005, A&A, 432, 401

Golombek, D., Miley, G. K., & Neugebauer, G. 1988, AJ, 95, 26

Gurwell, M. A., Peck, A. B., Hostler, S. R., Darrah, M. R., & Katz, C. A. 2007, From Z-Machines to ALMA: (Sub)Millimeter Spectroscopy of Galaxies, 375, 234

Hartman, R. C., et al. 1999, ApJS, 123, 79

Johnson, W. N., Zdziarski, A. A., Madejski, G. M., Paciesas, W. S., Steinle, H., & Lin, Y-C 1997, in AIP Conf. Proc. 410, Fourth Compton Symposium, ed. Dermer, C., Strickman, M., & Kurfess, J. (Woodbury, NY: AIP), 283

Kadler, M. 2005, PhD Thesis, University of Bonn, Bonn, Germany

Kadler, M., Ros. E., Perucho, M., et al., ApJ, in press (arXiv:0801.0617)

Kalberla, P. M. W., Burton, W. B., Hartmann, D., Arnal, E. M., Bajaja, E., Morras, R., Pöppel, W. G. L. 2005, A&A, 440, 775

Maisack, M., Mannheim, K., & Collmar, W. 1997, A&A, 319, 397

Michelson, P. F. 2007, in AIP #921, "The First GLAST Symposium", Melville, New York, 8

Ritz, S. 2007, in AIP #921, "The First GLAST Symposium", Melville, New York, 3

Sguera, V., Bassani, L., Malizia, A., Dean, A. J., Landi, R., & Stephen, J. B. 2005, A&A, 430, 107

Sreekumar, P., et al. 1992, ApJ, 400, L67

Sreekumar, P., Bertsch, D. L., Hartman, R. C., Nolan, P. L., & Thompson, D. J. 1999, Astroparticle Physics, 11, 221

Skrutskie, M. F., et al. 2006, AJ, 131, 1163

Thompson, D. J., et al. 1994, in "Multi-Wavelength Continuum Emission of AGN", ed. Courvoisier, T. J.-L., & Bleha, A., (The Netherlands: IAU), 49

Tueller, J., Mushotzky, R. F., Barthelmy, S., Cannizzo, J. K., Gehrels, N., Markwardt, C. B., Skinner, G. K., & Winter, L. M. 2007, ArXiv e-prints, 711, arXiv:0711.4130
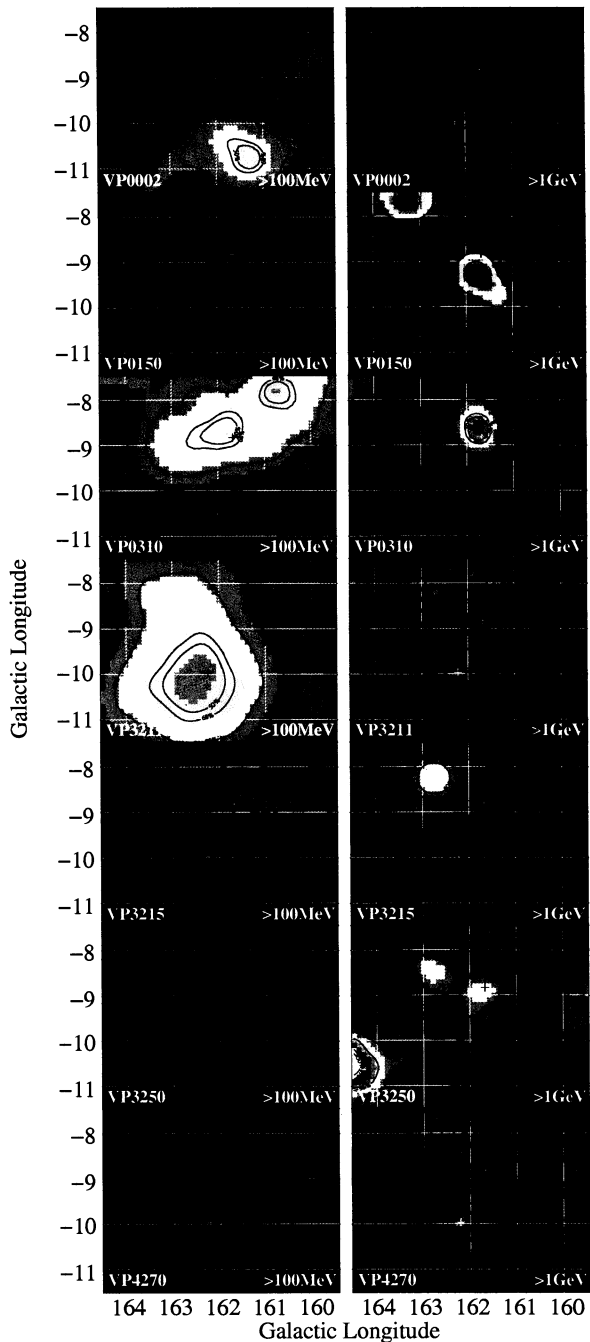
Fig. 1.— Likelihood maps for the seven viewing periods with TS>3 (anywhere in the map, either energy range). The left column panels are for E>100 MeV, while the right column panels show E>1000 MeV, with fewer photon but considerably smaller point spread function. Crosses show the positions of 3C 111 and 3EG J0416+3650; ref. Figure 2.
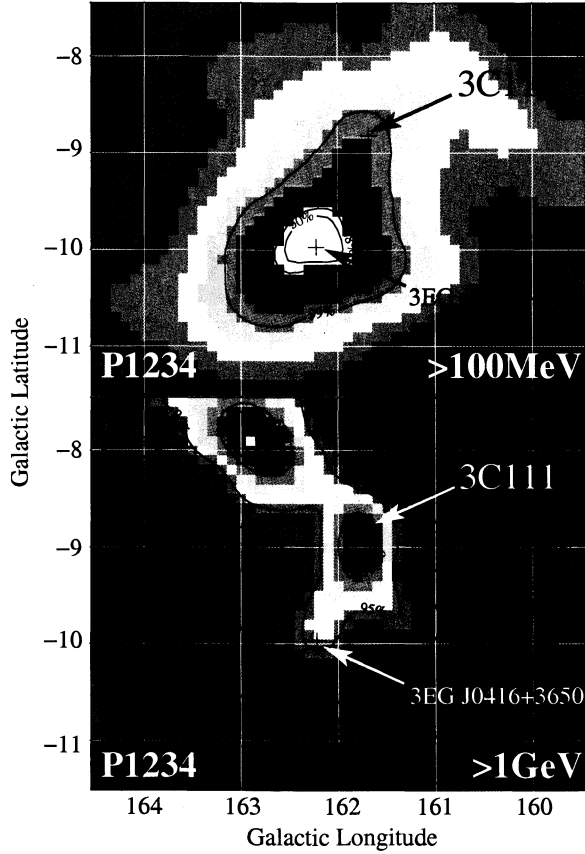
Fig. 2.— Likelihood maps for the summed exposure of all viewing periods, for >100 MeV (top) and >1000 MeV (bottom).
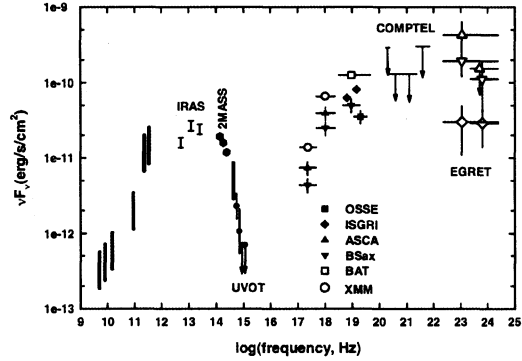

Fig. 3.— Spectral energy distribution for 3C 111. The data points are non-contemporaneous; their values and references are tabulated in Table 3. Thick vertical lines indicate historical ranges for radio and submillimeter observations. The thick vertical line in the optical indicates the range of R-band fluxes from 2004-2007 observations with the Liverpool Telescope - see text. The NIR through UV points have been dereddened; see text. For the EGRET data, the average value are indicated with open diamonds, the most significant single viewing period, VP0310, uses downward-pointing open triangles, and the maximum flux, VP3215, is shown with upward-pointing triangles. The lowest upper limit for a single VP (not shown) is similar to the average.
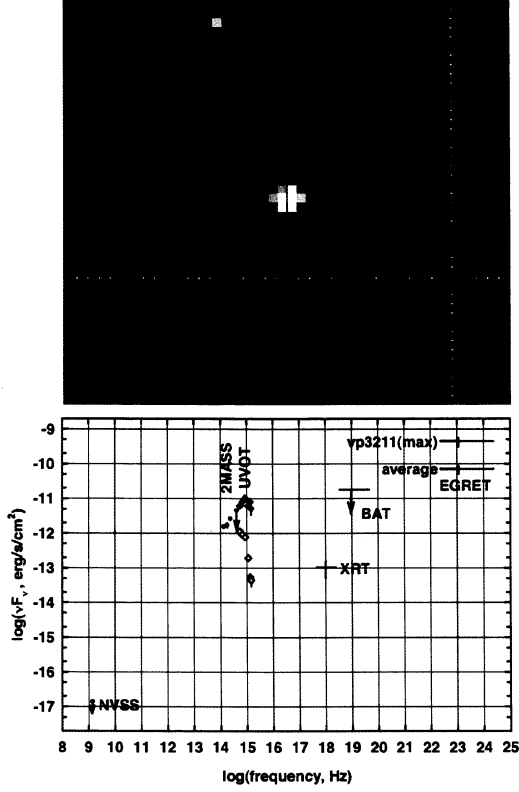
11

Fig. 4.— (a) UVOT image (UW1 filter) of the region around Swift J041554.3+364926. The circle indicates the position uncertainty of the X–ray source; (b) Spectral energy distribution for Swift J041554.3+364926. The data points are non-contemporaneous; their values and references are tabulated in Table 3. For the UVOT data points, the observed values are shown as open circles, while dereddened values are shown as filled circles. The EGRET values may not be associated with the lower-frequency source - see text.